RSC Advances

PAPER

View Article Online
View Journal | View Issue

Cite this: *RSC Adv.*, 2025, **15**, 7069

Synthesis and characterization of spin coated ZnTe thin films for improving the efficiency of ZnTe/ZnS solar cell using SCAPS-1D†

Md. Hasan Ali, *[ab] Md. Dulal Haque,[a] Md. Faruk Hossain[c] and Abu Zafor Md. Touhidul Islam*[d]

Cadmium telluride (CdTe) absorber layer in solar cells (SCs) is environmentally dangerous for the toxic behavior of cadmium (Cd). Alternatively, zinc telluride (ZnTe) is deliberated as a promising PV material for its adoptable absorption coefficient, better conversion efficiency and low production cost of materials requirements. The main objective of this study is to synthesis and characterization analysis of ZnTe thin films to enhance the performance of ZnS/ZnTe solar cell. The structural, optical, morphological and compositional properties of the ZnTe thin films were investigated by X-ray diffraction, UV-visible spectroscopy, scanning electron microscopy, and energy dispersive spectroscopy. The performance of the cell was analyzed by SCAPS-1D. The XRD results showed that all the spin coated ZnTe thin films are in cubic phase. The determining optical band gap values are in the range of 1.77–2.18 eV. The SEM images indicated that the surface of ZnTe thin film annealed at 400 °C has better surface coverage area with homogeneity, good uniformity, and minimum void compared to the other annealed samples. The EDS study exhibits that all the films are Te richness with p-type conductivity. The highest power conversion efficiency (PCE) is found 17.45% with V_{oc} of 1.41 V, J_{sc} of 14.01 mA cm^{-2} and FF of 88.53% for the 1184 nm optimum thickness of ZnTe and annealed at 400 °C. zinc sulfide (ZnS), indium tin oxide (ITO), platinum (Pt) and aluminum (Al) are indicated as buffer layer, transparent conductive oxide, back metal and front metal respectively of the device. All the findings confirmed that the deposited ZnTe thin films are suitable for usage as an absorber layer in thin film solar cells (TFSCs).

Received 17th January 2025
Accepted 25th February 2025

DOI: 10.1039/d5ra00417a

rsc.li/rsc-advances

1. Introduction

The combustion of conventional fossil fuels such as natural gas, oil and coal has caused substantial damage to the environment and global warming. As a result, sustainable and renewable energy demand is increasing rapidly due to the higher population growth rate, industrial usage, expansion of world economy, and the socio-economic pressure. Renewable energy sources have become as good alternative of conventional energy sources for their environmental qualities.[1] Among all of the renewable energy sources, solar energy is the most abundant, eco-friendly, clean, cost effective and long lasting way to address the growing global energy demand for resolving the humanity's energy crisis.[2,3] However the amount of produced solar energy is insufficient and not profitable. So, the researchers are interested in thin films solar cells (TFSCs) due to a smaller amount material usage, light weight, low priced, low processing costs, mechanical flexibility and lower energy requisites for production.[2,3]

Throughout the previous a couple years, group II–VI binary semiconductors (II = Zn, Cd, Hg and VI = S, Se, Te) have been broadly researched due to the outstanding structural, electrical and optical properties and extensively utilized in optoelectronic and photovoltaic devices.[4,5] Among II–VI semiconductors, CdTe has gained significant interest as an absorber layer in SCs and numerous researches are published their works for its potential PCE (18–24%).[6] But for the toxicity of Cd, it demonstrates environmental threat at the end of photovoltaic (PV) module lifetime.[7]

Recently, ZnTe has gained enormous attention from researchers owing to its adjustable direct band gap energy ranging from 1.7 to 2.4 eV at ambient temperature,[8] low electron affinity of 3.53 eV,[9] high absorption coefficient in the order of 10^4 cm^{-1},[10] high hole mobility of 80–100 cm^2 V^{-1} s^{-1},[11] with lattice constant of 6.103 Å.[12] Moreover, ZnTe is a most

[a]Department of Electronics and Communication Engineering, Hajee Mohammad Danesh Science and Technology University, Dinajpur-5200, Bangladesh
[b]Advanced Energy Materials and Solar Cell Research Laboratory, Department of Electrical and Electronic Engineering, Begum Rokeya University Rangpur, Rangpur-5400, Bangladesh. E-mail: hasan@brur.ac.bd
[c]Department of Electrical and Electronic Engineering, Rajshahi University of Engineering and Technology, Rajshahi-6204, Bangladesh
[d]Department of Electrical and Electronic Engineering, University of Rajshahi, Rajshahi-6205, Bangladesh. E-mail: touhid.eee@ru.ac.bd

† Electronic supplementary information (ESI) available. See DOI: https://doi.org/10.1039/d5ra00417a

promising brick-red color material with p-type conductivity, making it suitable for the advancement of efficient, low-cost SCs. Its abundance, environmental friendliness, ability to be deposited at lower temperatures, compatibility with various substrates, and excellent thermal durability further enhance its potential.[13] ZnTe exhibits two distinct structural forms. One is cubic or zinc blende structure and another is wurtzite or hexagonal structure. Cubic structure is found at room temperature with lattice constant $a = 6.104$ Å belongs to the space group of $F\overline{4}3\ m$.[14] Elsewhere, wurtzite structure is reveal at high pressure with lattice constant $a = 4.045$ Å and $c = 9.342$ Å belongs to the space group of $P3_1$.[15]

Because of excellent optical and electronic properties of ZnTe, many researchers have investigated ZnTe based solar cells to improve the performance. The PCE has been determined 1.86% of p-ZnTe/n-CdSe structure with J_{SC} of 11.60 mA cm^{-2}, V_{OC} of 0.415 V, and FF of 38.6%.[16] The 1.1% and 1.42% PCE have been measured for n-ZnO/i-ZnTe/p-ZnTe and ZnTe based homojunction solar cells correspondingly.[17] The theoretical PCE of 10% has been achieved for n-ZnO/n-CdS/p-ZnTe solar cell with 2000 nm thickness of ZnTe.[18] The 12.28% and 13.37% PCE have been recorded for without and with ZnTe back surface field (BSF) layer of n-ZnO/n-CdS/p-ZnTe structure.[19] The 9.2%, 10.6% and 17.8% PCE have been determined for ZnTe, Sb:ZnTe and Sn:ZnTe absorber materials respectively with 1500 nm absorber thickness.[20] The 16.5% practical PCE has been achieved for glass/ITO/p-ZnTe/n-ZnS/n-CdS/Au multi-junction solar cell.[13] Recently, the highest theoretical PCE of 18.40% and 20.20% have been determined for without and with In_2Te_3 BSF layer of glass/ZnO/CdS/ZnTe solar cell structure.[3]

Until now, there are numerous techniques have been utilized to fabricate ZnTe thin films. These techniques are RF sputtering,[21] electron beam evaporation,[12] thermal evaporation,[22] electro deposition,[5] physical vapor deposition (PVD),[23] chemical bath deposition (CBD),[24] physical vapor deposition coupled with glancing angle,[25] pulsed laser deposition (PLD),[26] closed space sublimation (CSS),[27] hydrothermal,[28] metal–organic chemical vapor deposition (MOCVD),[29] molecular beam epitaxy (MBE),[30] successive ionic layer absorption and reaction (SILAR),[31] and hot-wall evaporation.[32] Of all of these, spin coating is a very simple and easy as well as low cost technique to fabricate uniform film. Moreover, high quality film thickness can be precisely control by varying rotating speed and the viscosity of the solution. To the best of our understanding, thin films of ZnTe absorber layer have not yet been deposited by spin coating method through thiol amine solution processed. Therefore, ZnTe thin films have been deposited using the spin coating process for solar cells application.

The novelty of this research is to direct synthesis using thiol-amine co-solvent and deposit ZnTe thin films on glass substrates *via* simple, easy, and inexpensive spin coating process to investigate annealing effect on the structural, optical, morphological, and compositional properties of the ZnTe thin films. Therefore, the major goal of this study was to synthesize and deposit nontoxic ZnTe as a Cd-free absorber layer using spin coating process for improving the performance of ZnTe/ZnS TFSCs. We hope this research will be positively beneficial to the researchers in the field of photovoltaic technology.

In this study, we investigated the effect of annealing temperatures on the structural, optical, morphological, and compositional properties of spin coated ZnTe thin films as a layer of absorption for TFSCs applications. The prepared ZnTe thin films were examined using X-ray diffractometer, UV-vis. spectrophotometer, scanning electron microscope, and energy dispersive spectroscope to investigate the structural, optical, morphological, and compositional features respectively. Furthermore, the cell performance was investigated *via* SCAPS-1D simulator.

2. Experimental details

2.1 Substrates cleaning, materials and preparation of precursor solution

Initially, (1 × 1)-inch glass substrates were immerged into the piranha solution for 20 minutes to remove any kinds of impurities from the substrates surface. The piranha solution was made of sulfuric-acid (H_2SO_4) and hydrogen peroxide (H_2O_2) at a volume ratio of 4 : 1. Secondly, the glass substrates were more cleaned by 2-propanone (acetone) for 12 minutes, 2-propanol (IPA) for 12 minutes, and distilled water for 15 minutes using an ultra-sonic bath and thereafter using an air blower to dry. Finally, the cleaned substrates were dried at 80 °C for 15 minutes. The details substrate cleaning process is shown in Fig. S1.†

High purity (99.99%) of ZnTe powder, ethane-1, 2-dithiol, and ethylenediamine co-solvents were collected from Sigma Aldrich to make ZnTe precursor solution without any further modification.

To make the ZnTe precursor solution, at first thiol-amine solution was made using ethylenediamine and 1, 2-ethanedithiol at proportion of volume 10 : 1. After that, 2 wt% of the ZnTe powder was added with thiol-amine solution and magnetically stirrer at 400 rpm, 50 °C for 22 hours. For proper dissolution of ZnTe powder with thiol-amine solution, the solution was further magnetically agitated at 500 rpm, 80 °C for 10 hours. Finally the solution was ready to prepare thin films. The precursor solution preparation process is shown in Fig. S2.†

2.2 Deposition of ZnTe thin films

The precursor solution of ZnTe was deposited on cleaned glass substrates to create four ZnTe thin films *via* spin coating process. The rotational speed of spin coater was set to 500 rpm for 10 seconds and 3000 rpm for 50 seconds. Then the prepared ZnTe thin films have been pre-annealed at 100 °C for ten minutes using a hot plate to remove any leftover solvents. Now, the films are considered as as-deposited films. After that, three pre-annealed films have been further post-annealed at 200, 300, and 400 °C temperatures for 15 minutes using Nabertherm muffle furnace. The deposition and annealing process is shown in Fig. S3.†

2.3 Characterization of ZnTe thin films

The structural property of the synthesized ZnTe thin films was analyzed using Shimadzu, LabX XRD-6100 X-ray diffractometer. The Shimadzu UV-260 UV-vis. Spectrophotometer was used to measure the transmittance and absorbance spectra for analyzing optical properties of ZnTe thin films. The JEOL 6100 plus Scanning Electron Microscope (SEM) was used to investigate the surface morphological property of the ZnTe thin films. The Energy Dispersive Spectroscope (EDS) JCM-6000Plus model was used to determine the compositional analysis of ZnTe thin films.

3. Results and discussion

3.1 XRD study

Fig. 1 shows the XRD patterns of the as-deposited and annealed at 200, 300, and 400 °C temperature for the ZnTe thin films in the range of $2\theta = 20$–$80°$. The XRD patterns indicate that all the films have polycrystalline nature with zinc blende (cubic) structure. The highest intensity peak observed at closely $2\theta = 25.26°$ with preferred orientation along (111) plane that confirms the films are nano crystalline in nature. Two other lower intensity peaks are detected at $2\theta = 41.81°$ and $49.49°$ along with (220) and (311) planes respectively. According to the JCPDS card no. 00-015-0746, all three diffraction peaks conform that the ZnTe thin films are in cubic crystal structure.[33] It is noted that the peaks intensities increase with increasing the annealing temperature. As a result, the crystallite size enlarge with increasing the annealing temperature.[34]

The crystalline interrelated structural parameters like as interplanar spacing, lattice parameter, crystallite size, micro strain and dislocation density were determined from the XRD data using the eqn (1) to(5) and are listed in Table 1.

The interplanar spacing (d_{hkl}) was enumerated using the following Bragg's diffraction formula:

$$d_{hkl} = \frac{n\lambda}{2 \sin \theta_{hkl}} \quad (1)$$

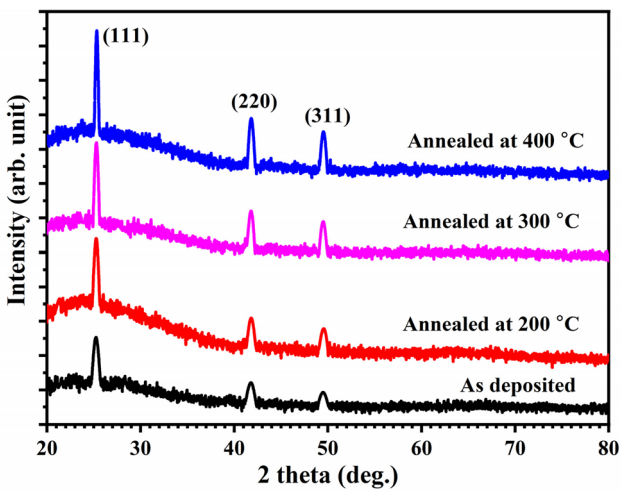

Fig. 1 XRD patterns of ZnTe thin film for as-deposited and annealed at 200, 300 and 400 °C temperature.

where, n is the reflection order usually equal to unity, λ is X-ray's wavelength (0.154056 nm) and θ_{hkl} is the diffraction angle of Bragg corresponding to (hkl) planes.

The perpendicular distance between two adjacent planes in a crystal is known as interplanar spacing. From Table 1 it is seen that, the interplanar spacing value slightly decreased with increasing annealing temperature which could be ascribed to further grains realignment and the significance annealing induced robust relationship between the vapor atoms and the substrate.[35] The calculated interplanar spacing values are close match with[36,37] and JCPDS card no. 015-0746.

The lattice parameter for the cubic phase of ZnTe structure was determined by the following relation:[38]

$$a = d_{hkl} \sqrt{(h^2 + k^2 + l^2)} \quad (2)$$

The lattice parameter value is slightly decreased with increasing the annealing temperature due to the higher crystallite size at higher heat-treated. Furthermore, the 2θ peak position of the most dominant (111) plane is a bit moved towards higher side with increasing the annealing temperature as in.[36] The determined lattice parameter values are well matched with previous articles[36,39,40] and JCPDS card no. 015-0746.

The ZnTe thin film's crystallite size (D) was ascertained from the Debye–Scherer formula:[41]

$$D = \frac{0.9\ \lambda}{\beta \cos \theta} \quad (3)$$

where, β represents full width at half maximum (FWHM).

The narrowness, sharpness and intensity of the diffraction peaks are increased with increasing annealing temperature which clarifies the improvement of crystallinity in the films with increasing the annealing temperature. Similar fashion of increment in sharpness and intensity of the diffraction peaks with increasing annealing temperature are found in (ref. 36,42). The crystallite size increases with decreasing the FWHM. The XRD analysis reveal that the average crystallite size are 15.42 nm, 17.84 nm, 20.31 nm, and 25.26 nm for the as-deposited and annealed at 200, 300, and 400 °C of ZnTe thin films, respectively. The films at higher annealing temperature exhibit more enhancements in intensity and crystallinity than lower heat treated film. As a result, the size of the crystallite increased as the annealing temperature increased.

The micro strain (ε) was ascertained by the Stoke and Wilson equation:[39]

$$\varepsilon = \frac{\beta}{4 \tan \theta} \quad (4)$$

It is clear from Table 1 that the FWHM values decreases with increasing the annealing temperature. As a result, the micro strain values decrease with increasing the annealing temperature because micro strain is directly proportional to the FWHM. The average micro strain values are 7.181×10^{-3}, 6.199×10^{-3}, 5.461×10^{-3}, and 4.434×10^{-3} for the as-deposited and annealed at 200, 300, and 400 °C ZnTe thin films,

Table 1 Structural related parameters of ZnTe thin films

Samples	2θ (°)	Plane (*hkl*)	FWHM (°)	*d* (Å)	*a* (Å)	*D* (nm)	Micro strain, $\varepsilon \times 10^{-3}$	Dislocation density $\delta \times 10^{15}$(lines per m^2)
As-deposited	25.22	111	0.4235	3.528	6.111	19.22	8.260	2.707
	41.81	220	0.6053	2.159	6.106	14.05	6.915	5.066
	49.49	311	0.6728	1.840	6.103	13.00	6.369	5.917
Annealed at 200 °C	25.26	111	0.3831	3.523	6.102	21.25	7.460	2.215
	41.81	220	0.5083	2.159	6.105	16.73	5.806	3.573
	49.49	311	0.5632	1.840	6.103	15.53	5.332	4.146
Annealed at 300 °C	25.28	111	0.3112	3.520	6.097	26.16	6.055	1.461
	41.81	220	0.4727	2.158	6.104	17.99	5.398	3.090
	49.50	311	0.521	1.840	6.102	16.79	4.931	3.547
Annealed at 400 °C	25.32	111	0.2349	3.515	6.087	34.66	4.563	0.832
	41.82	220	0.4014	2.158	6.104	21.19	4.584	2.227
	49.50	311	0.4391	1.840	6.102	19.92	4.156	2.520

correspondingly. The obtained micro strain values are good agreement with earlier reports.[42,43]

Using the Williamson and Smallman's relation, dislocation density (δ) was ascertained from following formula:[44]

$$\delta = \frac{1}{D^2} \quad (5)$$

Generally larger crystallite size or smaller FWHM specify the existence of lower degree of defects and dislocation densities. The average dislocation density are found 4.563×10^{15} lines per m^2, 3.311×10^{15} lines per m^2, 2.699×10^{15} lines per m^2, and 1.860×10^{15} lines per m^2 for the as-deposited and annealed at 200, 300, and 400 °C films, respectively.

The diminution of micro strains and dislocation density with increasing the annealing temperature which perhaps due to the decrease of grain boundaries.[42] The amounts of lattice defects decreased with increasing the annealing temperature because of the crystallite size improvement with increasing annealing process.[45,46]

3.2 Optical properties

The optical characteristics of the as-deposited and annealed at various (200–400) °C temperatures of the ZnTe thin films were investigated *via* UV-vis. spectrophotometer. Fig. 2 shows the changing of optical absorbance spectra of the as-deposited and annealed at various temperatures of the ZnTe thin films between 300–900 nm wavelengths. The absorbance spectra show decreasing nature for all the samples with increasing the wavelength but the absorbance increased with increasing the annealing temperature. The decreasing fashion of absorbance with increasing of wavelength may result from a band to band electronic transition between conduction band and ionization donor level.[47,48] The high absorption at higher annealing temperature which may causes of the increasing of Zn concentration and decreasing of Te concentration on the surface of the film. This is verified by the compositional analysis (EDS) in Section 3.4.

Fig. 3 shows the changing of transmittance of all ZnTe thin films. The transmittance varies with wavelength in accordance with the related absorbance spectra. The transmittance of the all samples increases with increasing the wavelength but the transmittance is lower at higher annealing temperature. The average transmittance in the visible range of the as-deposited and annealed at 200, 300, and 400 °C films are found 8.96%, 5.47%, 4.75% and 2.75%, respectively. The minimum transmittance is found at higher annealing temperature (400 °C) because of the lower existence of Te element, which is the potential optical absorption factor.[12] On the other hand, the growth of crystal and the crystallite size improvement possibly accountable for the lower transmittance at higher annealing temperature.[45,49,50] The lower transmittance and higher absorbance at lower wavelength (at higher photon energy) makes the ZnTe thin films for better use as an absorber layer in thin film solar cells. The similar fashion of absorbance and transmittance are found in the previous published articles.[12,36,43]

The optical absorption coefficient (α) of the ZnTe thin films was calculated by the following relation:[27]

$$\alpha = \frac{1}{t}\ln\left(\frac{1}{T}\right) \quad (6)$$

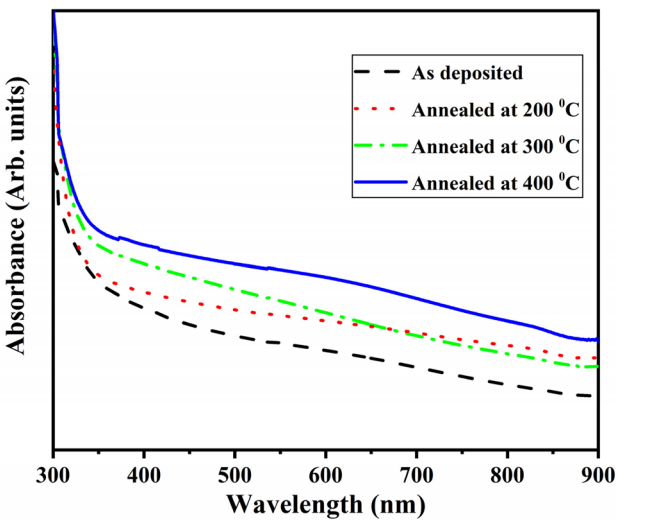

Fig. 2 The variation of optical absorbance spectra of the as-deposited and annealed at various temperatures of the ZnTe thin films with wavelengths.

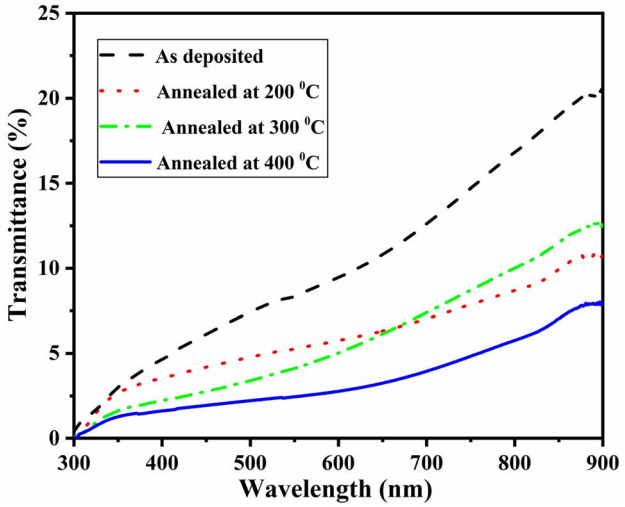

Fig. 3 The variation of optical transmittance spectra of the as-deposited and annealed at various temperatures of the ZnTe thin films with wavelengths.

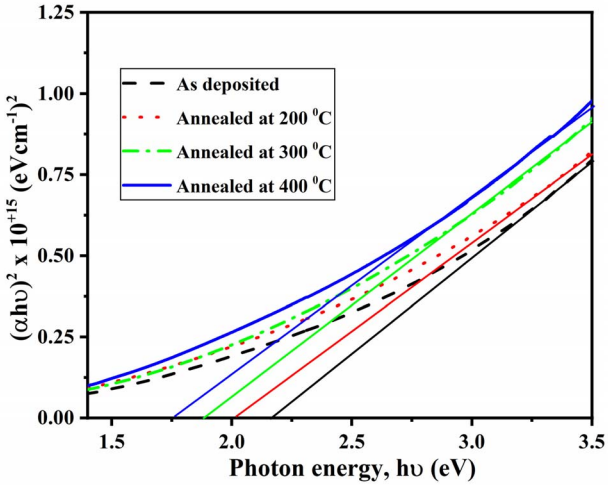

Fig. 4 Tauc plot for as-deposited and annealed at 200, 300, and 400 °C temperature of ZnTe thin films.

where, t and T is the thickness and transmittance of the films, respectively.

The changing of the energy dependent absorption coefficient (α) in the fundamental absorption segment related with the incident photon energy ($h\nu$) can be express by the following Tauc's formula:[51]

$$(\alpha h\nu) = A(h\nu - E_g)^{\frac{1}{2}} \quad (7)$$

where, h is Planck's constant, ν is incident photon frequency, A is a constant correlated to the effective masses of valence and conduction band and E_g is energy band gap.

Fig. 4 shows $(\alpha h\nu)^2$ *vs.* $(h\nu)$ plots of the as-deposited and annealed at 200, 300, and 400 °C temperature of ZnTe thin films. The direct band gap energy values were determined from the extrapolation of linear segment of $(\alpha h\nu)^2$ and $(h\nu)$ plots at zero of absorption coefficient. The estimated band gap values of the ZnTe thin films are 2.18 eV, 2.03 eV, 1.90 eV and 1.77 eV for the as-deposited and annealed at 200, 300, and 400 °C temperature, respectively. The estimated band gap values are well matched with the previous published articles.[5,50,52,53] The determined band gap values of ZnTe are a bit lower than the value of 2.26 eV.[54] The band gap values decrease with increasing the annealing temperature due to the presence of Te element which introduces a significant fraction of electronic levels in the band gap close to the valence band edge of ZnTe with a consequent diminution of the energy related with the direct transition.[55,56] The variations of band gap from 2.18 eV to 1.77 eV possibly because of the elemental diffusion into the films at higher annealing temperature.[56] Furthermore, the band gap values reduce with rising the annealing temperature for the improvement of crystallite size of the deposited films.[5] The higher absorbance and lower transmittance at lower wavelength (at higher photon energy) as well as the exhibited band gap values makes the ZnTe thin films use as a layer of absorption in SCs application.

The absorption coefficient of the as-deposited and annealed at 200, 300, and 400 °C temperature of ZnTe thin films as shown in Fig. 5. From Fig. 5 observed that the sharp decreases of absorption coefficient in the UV region and slow decreases in the visible range with increasing the wavelength. The absorption coefficient values are within the order of 10^4 cm^{-1} for all the samples. But at higher annealing temperature the absorption coefficient value is higher than the other samples.

3.3 SEM study

Scanning electron microscope (SEM) technique is used to analyze surface morphological features of ZnTe thin films. The surface morphological images for the as deposited and annealed at 200, 300, and 400 °C temperature of ZnTe thin films are shown in Fig. 6(a)–(d), respectively. From the figure of micrograph, the ZnTe thin film annealed at 400 °C temperature has most excellent surface coverage area with good uniform

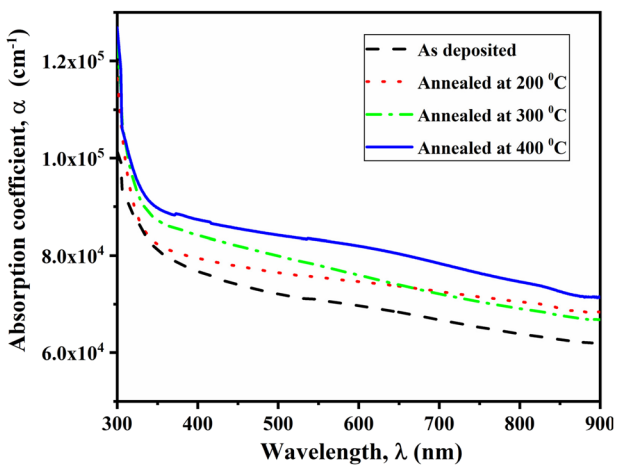

Fig. 5 Change in absorption coefficient of as-deposited and annealed at 200, 300, and 400 °C temperature of ZnTe thin films.

morphology. So, it can be decided that the ZnTe thin film's surface annealed at 400 °C temperature has highly smooth, uniform and homogeneous with lowest amount of pinholes, void, and cracks compared among the other samples. The SEM images expose smooth ordination of grains with varying sizes. In Fig. 6(d), the largest grain size is observed at 400 °C annealed temperature in the ZnTe film. This remark is correlated with XRD result, which specifies the maximum peak intensity at 400 °C annealed temperature in the ZnTe film.[57]

3.4 EDS study

The presence of Zn and Te atoms in the as-deposited and annealed at 200, 300, and 400 °C temperature for the ZnTe thin films have been determined from energy dispersive spectroscopy (EDS) technique. Table 2 represents the elemental composition of Zn and Te elements in ZnTe thin films. The presence of Zn and Te atoms in the thin films confirmed that the successful formation of ZnTe films.

From Table 2 it is clear that all the ZnTe films have excess Te over Zn. So, the resulting films are classified as p-type ZnTe because of richness of Te than Zn in every film[43,53] and could be used as potential absorber layer for thin film solar cells. Since, Zn and Te have different vapor pressures, therefore the deposited films are Te rich and higher annealed film approaches towards nearly stoichiometric nature. As the annealing temperature increases, the composition of the % of the Zn atoms increased from 37.24 to 42.83% while the % of Te atoms decreased from 62.76 to 57.17% and the ratio of Zn to Te atoms attained close to the stoichiometric ratio of 1 : 1. The stoichiometric ratio may be further optimizing by adjusting the deposition conditions. The composition of Zn in ZnTe thin films increased from 37.24% to 42.83% with increasing the annealing temperature which may be the probable reasons for reduction of band gap with increasing the annealing temperature in ZnTe thin films for the metallic behavior of Zn.[53]

Table 2 Elemental compositions of Zn and Te in ZnTe thin films

	Elements (at%)		
Samples	Zn	Te	Zn : Te
As-deposited	37.24	62.76	1 : 1.7
Annealed at 200 °C	38.24	61.76	1 : 1.6
Annealed at 300 °C	39.08	60.92	1 : 1.5
Annealed at 400 °C	42.83	57.17	1 : 1.3

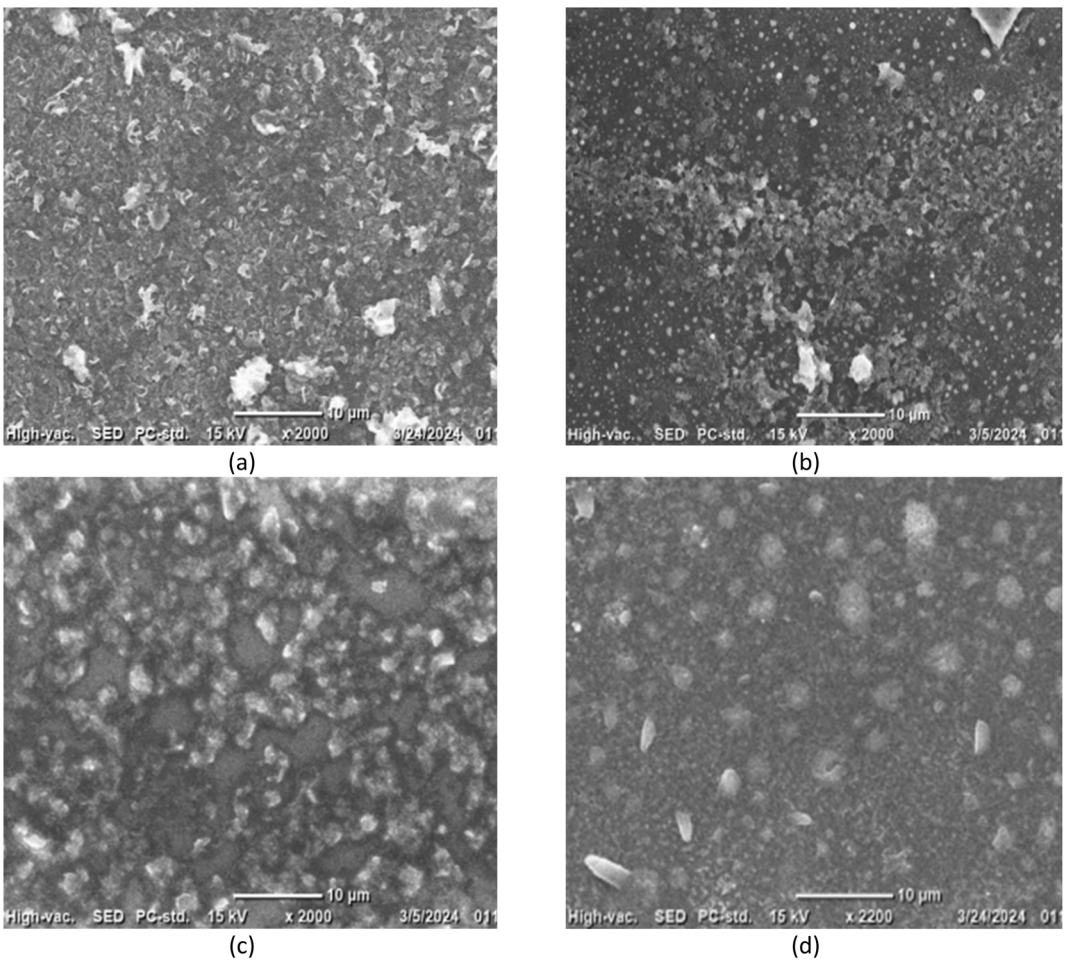

Fig. 6 SEM images of ZnTe thin films for (a) as-deposited and annealed at (b) 200, (c) 300, and (d) 400 °C temperature.

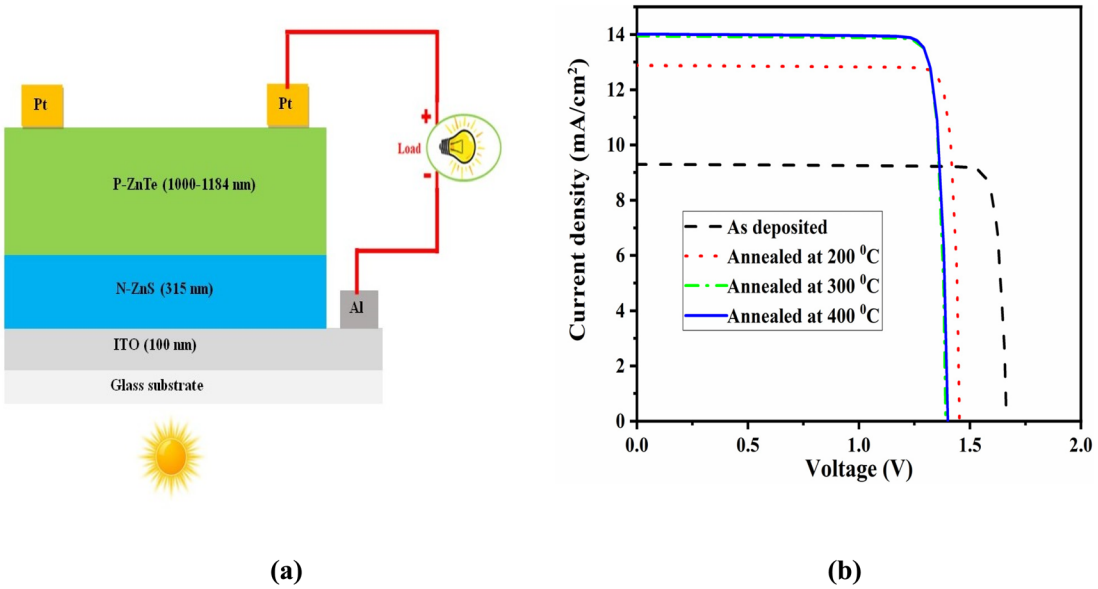

Fig. 7 (a) the schematic structure of the cell and (b) *J–V* curve of as deposited and annealed at 200, 300, and 400 °C temperatures of ZnTe thin films.

3.5 Performance of ZnS/ZnTe solar cell

SCAPS-1D simulator is used to analyze the performance of ZnS/ZnTe solar cell with one sun (1000 W m^{-2}) illumination and global air mass of 1.5 G lunar band. One dimensional fundamental model of semiconductor was used to build SCAPS-1D under steady-state conditions together with Poisson's (eqn (8)) and continuity (eqn (9)) & (eqn (10)) equations for holes and electrons respectively.

$$\frac{d^2\psi}{dx^2} = -\frac{q}{\varepsilon}\left(p - n + N_d{}^+ - N_A{}^- + \frac{\rho_{def}}{q}\right) \quad (8)$$

$$-\frac{1}{q}\frac{dJ_p}{dx} = G - R_p \quad (9)$$

$$\frac{1}{q}\frac{dJ_n}{dx} = G - R_n \quad (10)$$

where, ψ is electrostatic potential, q is charge of electron, $\varepsilon = (\varepsilon_0\varepsilon_r)$ is dielectric permittivity, ε_0 and ε_r are dielectric permittivity of free space and semiconductor, n and p are free carrier concentration of electron and hole, NA− and Nd+ are ionized acceptor and donor density, ρ_{def} is charge defect density, J_p and J_n are hole and electron current density, G is the generation rate, R_p and R_n are the recombination rate of hole and electron respectively.

The Poisson and continuity equations allow to model physical and electronic structure of TFSCs by signifying every layer's electrical and optical parameters used in the simulation. The transportation of electrons and holes is specified by (eqn (11)) and (eqn (12)) correspondingly.

$$J_n = -qD_n\frac{dn}{dx} + q\mu_n\frac{d\psi}{dx} \quad (11)$$

$$J_p = -qD_p\frac{dp}{dx} - q\mu_p\frac{d\psi}{dx} \quad (12)$$

Here, D_n and D_p are the diffusion coefficient of electron and hole, μ_n and μ_p are the mobility of electron and hole respectively.

The thickness (315 nm), band gap (3.80 eV), and transmittance of ZnS have been taken from,[58] and others parameters of ZnS have been taken from.[59,60] The measured thickness (1000–1184 nm) and band gap (1.77–2.18 eV) of ZnTe was varied to get the output of cell parameters. The others parameters of ZnTe have been taken from.[18,19] The defect density of ZnS and ZnTe layer was taken 1.0 × 10^{16} cm^{-3} and ZnS/ZnTe interface defect density was taken 1.0 × 10^{12} cm^{-2}. The schematic structure of the ZnTe/ZnS solar cell and current density–voltage (*J–V*) characteristic curve of ZnS/ZnTe hetero-junction solar cell is shown in Fig. 7(a) and (b), respectively. Table 3 represents the

Table 3 The output performance of ZnS/ZnTe solar cell

Samples	ZnTe film's thickness (nm)	Band gap (eV)	V_{oc} (V)	J_{sc} (mA cm^{-2})	FF (%)	PCE (%)
As-deposited	1000	2.18	1.67	9.30	90.41	14.01
Annealed at 200 °C	1119	2.03	1.46	12.89	89.83	16.90
Annealed at 300 °C	1165	1.90	1.40	13.94	89.39	17.42
Annealed at 400 °C	1184	1.77	1.41	14.01	88.53	17.45

output cell parameters of ZnS/ZnTe solar cell with the changes of thickness and band gap of the respective ZnTe thin films.

From Fig. 7(b) and Table 3 it is seen that the short circuit current density increased with increasing the annealing temperature of the samples due to the higher absorption and thickness of the ZnTe films. The open circuit voltage decreased due to the decreasing the measured band gap of the films with increasing the annealing temperature. The FF value decreased from 90.41–88.53% because of increasing the thickness of the films with increasing the annealing temperature. The highest 17.45% PCE is found with V_{oc} of 1.41 V, J_{sc} of 14.01 mA cm^{-2} and FF of 88.53% annealed at 400 °C film. Although previous experimental and theoretical study exhibits the PCE increases from 1.1% to 20.20% for the different structure and thickness of ZnTe absorber layer. It has been observed from Table 3, that the decrease of the band gap from 2.18 to 1.77 eV enables to absorb the lower energy photons in the visible range which contribute to increase the efficiency although the open circuit voltage reduces. The enhancement of the current due to the large number of photons absorption is represented in Fig. 7(b). The optimized band gap and thickness of ZnTe is considered 1.77 eV and 1184 nm, respectively from the experimental data to get highest performance of the ZnTe/ZnS solar cell.

4. Conclusion

In this research, ZnTe thin films were deposited using simple, easy and inexpensive spin coating technique on glass substrates. XRD, UV-visible spectrometry, SEM and EDS were used to analyze the effect of annealing temperature on structural, optical, morphological, and compositional properties of the ZnTe thin films. Furthermore, the ZnS/ZnTe cell performance was investigated using SCAPS-1D simulator. XRD results confirmed that the growths of excellent ZnTe thin films are cubic structure. The average transmittances in the visible range of the all films are in the range of 2.75–8.96%. The determined band gap values are found in between 1.77 to 2.18 eV. SEM micrograph provides good surface coverage area with homogeneity, and minimum cracks at higher annealing temperature. Compositional analysis confirmed that all films are richness of Te with p-type conductivity. Annealed at 400 °C film exhibits better performance with PCE of 17.45%, V_{oc} of 1.41 V, J_{sc} of 14.01 mA cm^{-2} and FF of 88.53% than the others films due to the better absorbance and highest thickness. This study signifies a new research guideline for non-toxic, cost effective and higher PCE of ZnTe based TFSCs.

Data availability

The data that has been used is confidential. The data will be available on reasonable request to the corresponding author(s).

Author contributions

Md. Hasan Ali- conceived, designed, and performed the solution preparation, film deposition, and data acquisition, analyzed and interpreted the data, performed the simulation, prepared all figures, wrote and reviewed the manuscript. Md. Dulal Haque- conceived, supervised, designed and reviewed the manuscript. Md. Faruk Hossain-conceived, acquired the data and reviewed the manuscript. Abu Zafor Md. Touhidul Islam-conceived, supervised, and reviewed the manuscript.

Conflicts of interest

There are no conflicts of interest among the authors which have been declared by the statement.

Acknowledgements

The authors declare that this research did not receive any specific grant from funding agencies in the public, commercial, or not-for-profit sectors.

References

1 A. A. Faremi, A. T. Akindadelo, M. A. Adekoya, A. J. Adebayo, A. O. Salau, S. S. Oluyamo and P. A. Olubambi, *Results Eng.*, 2022, **16**, 100622.
2 M. Bošnjaković, R. Santa, Z. Crnac and T. Bošnjaković, *Sustainability*, 2023, **15**, 11888.
3 M. H. Ali, M. D. Haque, M. M. Hossain and A. Z. M. T. Islam, *J. Appl. Electrochem.*, 2024, **54**, 1013–1031.
4 B. H. AlMaiyaly, B. H. Hussein and A. H. Shaban, *J. Phys.: Conf. Ser.*, 2018, **1003**, 012084.
5 M. I. Hossain, M. Kamruzzaman and A. B. M. Obaidul Islam, *J. Mater. Sci.: Mater. Electron.*, 2015, **26**, 1756–1762.
6 M. A. Green, E. D. Dunlop, J. Hohl-Ebinger, M. Yoshita, N. Kopidakis, K. Bothe, D. Hinken, M. Rauer and X. Hao, *Prog. Photovoltaics Res. Appl.*, 2022, **30**, 687–701.
7 F. Li, S. Shaw, C. Libby, N. Preciado, B. Bicer and G. Tamizhmani, *Waste Manag.*, 2024, **174**, 646–665.
8 G. I. Rusu, P. Prepelita, N. Apetroaei and G. Popa, *J. Optoelectron. Adv. Mater.*, 2005, **7**, 829–835.
9 A. Pistone, A. S. Arico, P. L. Antonucci, D. Silvestro and V. Antonucci, *Sol. Energy Mater. Sol. Cells*, 1998, **53**, 255–267.
10 I. Lungu, V. V. Zalamai, E. I. Monaico, L. Ghimpu and T. Potlog, *J. Mater. Sci.*, 2023, **58**, 4384–4398.
11 K. Kumari, A. Jana, A. Dey, T. Chakrabarti and S. K. Sarkar, *Opt. Mater.*, 2021, **111**, 110574.
12 D. Suthar, Himanshu, S. L. Patel, S. Chander, M. D. Kannan and M. S. Dhaka, *Solid State Sci.*, 2020, **107**, 106346.
13 E. Shalaan, E. Ibrahim, F. Al-Marzouki and M. Al-Dossari, *Appl. Phys. A:Mater. Sci. Process.*, 2020, **126**, 852.
14 F. J. Ochoa-Estrella, A. Vera-Marquina, I. Mejia, A. L. Leal-Cruz, M. I. Pintor-Monroy and M. Quevedo-López, *J. Mater. Sci.: Mater. Electron.*, 2018, **29**, 20623–20628.
15 K. Kusaba and D. J. Weidner, *AIP Conf. Proc.*, 2008, **553**, 553–556.
16 N. G. Patel, C. J. Panchal, K. K. Makhija, P. G. Patel and S. S. Patel, *Cryst. Res. Technol.*, 1994, **29**, 247–252.
17 T. Tanaka, M. Miyabara, K. Saito, Q. Guo, M. Nishio, K. M. Yu and W. Walukiewicz, *Mater. Sci. Forum*, 2013, **750**, 80–83.

18 O. Skhouni, A. El Manouni, B. Mari and H. Ullah, *EPJ Appl. Phys.*, 2016, **74**, 1–6.
19 H. Bayad, A. El Manouni, B. Marí, Y. H. Khattak, S. Ullah and F. Baig, *Opt. Quantum Electron.*, 2018, **50**, 259.
20 P. Chamola and P. Mittal, *Optik*, 2020, **224**, 165626.
21 T. Kim, Y. Kim and I. Lee, *Nanotechnol. Accept.*, 2017, **30**, 13LT01.
22 K. M. Ur Rehman, X. Liu, M. Riaz, Y. Yang, S. Feng, M. W. Khan, A. Ahmad, M. Shezad, Z. Wazir, Z. Ali, K. M. Batoo, S. F. Adil, M. Khan and E. H. Raslan, *Phys. B:Condens. Matter*, 2019, **560**, 204–207.
23 Y. Wang, H. Li, T. Yang, Z. Zou, Z. Qi, L. Ma and J. Chen, *Mater. Lett.*, 2019, **238**, 309–312.
24 I. A. Younus, A. M. Ezzat and M. M. Uonis, *Nanocomposites*, 2020, **6**, 165–172.
25 R. Zarei, M. H. Ehsani and H. R. Dizaji, *Mater. Res. Express*, 2020, **7**, 026419.
26 T. I. Faydh, K. D. Salim and K. H. Mahmood, *J. Pharm. Negat. Results*, 2022, **13**, 214–217.
27 N. A. Shah and W. Mahmood, *Thin Solid Films*, 2013, **544**, 307–312.
28 B. B. Wang, M. K. Zhu, H. Wang and G. B. Dong, *Opt. Mater.*, 2011, **34**, 42–47.
29 Z. Li, J. Salfi, C. De Souza, P. Sun, S. V. Nair and H. E. Ruda, *Appl. Phys. Lett.*, 2010, **97**, 3–6.
30 E. Ozceri and E. Tarhan, *Appl. Phys. A:Mater. Sci. Process.*, 2019, **125**, 1–9.
31 S. S. Kale, R. S. Mane, H. M. Pathan, A. V. Shaikh, O. S. Joo and S. H. Han, *Appl. Surf. Sci.*, 2007, **253**, 4335–4337.
32 Y. M. Yu, S. Nam, J. K. Rhee, O. Byungsung, K. S. Lee and Y. D. Choi, *J. Cryst. Growth*, 2000, **210**, 521–526.
33 S. Rajpal and S. R. Kumar, *Solid State Sci.*, 2020, **108**, 106424.
34 S. Kavadiya, J. Strzalka, D. M. Niedzwiedzki and P. Biswas, *J. Mater. Chem. A*, 2019, **7**, 12790–12799.
35 S. Lalitha, R. Sathyamoorthy, S. Senthilarasu, A. Subbarayan and K. Natarajan, *Sol. Energy Mater. Sol. Cells*, 2004, **82**, 187–199.
36 R. H. Athab and B. H. Hussein, *Chalcogenide Lett.*, 2023, **20**, 477–485.
37 A. S. Nazar, A. A. Sayed and A. Murrawat, *J. Mater. Sci. Eng.*, 2017, **6**, 388.
38 B. D. Cullity, *Elements Of X-Ray Diffraction*, Addison- Weskey Publishing Company, Inc., London, 2nd edn, 1978.
39 M. Ahmed, A. Alshahrie and E. R. Shaaban, *Materials*, 2023, **16**, 3082.
40 J. R. Rathod, H. S. Patel, K. D. Patel and V. M. Pathak, *Adv. Mater. Res.*, 2013, **665**, 254–262.
41 B. D. Cullity, *Elements Of X-Ray Diffraction*, Addison-Weskey Publishing Company, Inc., London, 1972.
42 D. Suthar, Himanshu, S. L. Patel, S. Chander, M. D. Kannan and M. S. Dhaka, *Solid State Sci.*, 2020, **107**, 106346.
43 D. Suthar, Himanshu, S. L. Patel, S. Chander, M. D. Kannan and M. S. Dhaka, *J. Mater. Sci.:Mater. Electron.*, 2021, **32**, 19070–19082.
44 G. K. Williamson and R. E. Smallman, *Philos. Mag.*, 1956, **1**, 34–46.
45 H. Singh, N. Duklan, T. Singh, A. Thakur and J. Sharma, *J. Mater. Sci.:Mater. Electron.*, 2018, **29**, 4992–4998.
46 K. Ou, S. Wang, L. Bai, Y. Wang, K. Zhang and L. Yi, *Thin Solid Films*, 2019, **669**, 247–252.
47 A. Purohit, S. Chander, A. Sharma, S. P. Nehra and M. S. Dhaka, *Opt. Mater.*, 2015, **49**, 51–58.
48 S. Chander and M. S. Dhaka, *Phys. E*, 2016, **84**, 112–117.
49 S. N. Vidhya, O. N. Balasundaram and M. Chandramohan, *Optik*, 2015, **126**, 5460–5463.
50 A. B. Kashyout, A. S. Aricò, P. L. Antonucci, F. A. Mohamed and V. Antonucci, *Mater. Chem. Phys.*, 1997, **51**, 130–134.
51 P. Makuła, M. Pacia and W. Macyk, *J. Phys. Chem. Lett.*, 2018, **9**, 6814–6817.
52 A. E. Rakhshani, *Thin Solid Films*, 2013, **536**, 88–93.
53 O. I. Olusola, M. L. Madugu, N. A. Abdul-Manaf and I. M. Dharmadasa, *Curr. Appl. Phys.*, 2016, **16**, 120–130.
54 T. Mahalingam, V. S. John, S. Rajendran and P. J. Sebastian, *Semicond. Sci. Technol.*, 2002, **17**, 465–470.
55 T. Mahalingam, V. S. John, S. Rajendran, G. Ravi and P. J. Sebastian, *Surf. Coat. Technol.*, 2002, **155**, 245–249.
56 S. Shanmugan and D. Mutharasu, *Medziagotyra*, 2012, **18**, 107–111.
57 O. I. Olusola, M. L. Madugu and I. M. Dharmadasa, *Mater. Res. Innovations*, 2015, **19**, 497–502.
58 H. Ali, D. Haque, F. Hossain and M. Hossain, *J. Sol-Gel Sci. Technol.*, 2024, **110**, 560–566.
59 S. R. Al Ahmed and J. Ferdous, *IOP SciNotes*, 2020, **1**, 024802.
60 E. L. Ghyati Nabil, C. Meriem, M. Abdehadi, M. Abderahman, el mouden Mahmoud and E. Moznine reddad, *Mater. Today: Proc.*, 2022, **66**, 95–99.